中国激光

全固态单纵模273 nm深紫外激光器研制

窦微[1]，侯珊珊[1]，郑志远[1]，于博威[1]，陈曦[1]，郑权[1,2*]

[1]长春新产业光电技术有限公司，吉林 长春 130103；

[2]中国科学院长春光学精密机械与物理研究所，吉林 长春 130033

摘要 设计了一种稳定的单纵模273 nm深紫外激光器。采用输出功率为3.5 W、π偏振方向的444 nm激光二极管（LD）与σ偏振方向的441 nm LD的偏振合光作为泵浦源，端面泵浦长度为7 mm的Pr^{3+}:$LiYF_4$晶体，同时使用长度为5 mm的β-BaB_2O_4（BBO）晶体进行腔内倍频，利用法布里-珀罗（F-P）标准具进行单纵模的选取。当LD输出总功率为6240 mW时，可获得功率为32 mW的单纵模273 nm深紫外激光稳定输出。测量结果表明：光谱线宽小于80 fm，1 h均方根（RMS）功率稳定性优于1%。本研究方案在光生物学、半导体检测等领域具有较高的应用价值。

关键词 激光器；深紫外激光器；单纵模；Pr^{3+}:$LiYF_4$晶体；法布里-珀罗标准具

中图分类号 TN248.1 **文献标志码** A **DOI**：10.3788/CJL230524

1 引 言

深紫外光具有单光子能量高、波长短、更容易被材料吸收的特点，已被广泛应用于高密度光数据存储、高分辨率光学显微分析、材料处理、光谱分析、科研、医疗杀菌及诊断等领域[1-4]。近些年来，国内外学者及研究机构掀起了研究深紫外激光器的热潮。当前，大部分深紫外激光是对近红外激光进行两次非线性频率变换获得的，即：先通过二次谐波（SHG）技术将近红外激光转换成可见激光，再通过一次倍频或和频的方法获得深紫外激光。2004年，Sakuma等[5]使用布儒斯特切割的$CsLiB_6O_{10}$倍频9.6 W绿光激光器，获得了5 W连续266 nm激光。2006年，Wang等[6]使用$CsLiB_6O_{10}$四倍频Nd:YAG激光器获得了28.4 W 266 nm深紫外激光。2020年，赵彪等[7]采用Ⅰ类角度匹配的BBO晶体腔外倍频全固态单频532 nm激光器，获得了最大功率为810 mW的连续单频266 nm深紫外激光。此外，还有243 nm[8]、236.5 nm[9]、215 nm[10]等深紫外激光的报道。但是，利用近红外激光进行两次或多次非线性频率变换获得深紫外激光的方式，效率普遍较低。

近年来，一种可以在室温下直接输出可见光的稀土元素离子——三价镨离子（Pr^{3+}）备受关注，它的发射波长覆盖蓝光（485 nm）、绿光（523 nm）、橙光（604、607 nm）、红光（640、698、721 nm）等区域[11-12]。三价镨离子的出现也使得通过一次非线性频率变换获得深紫外激光的方法成为可能。2008年，相干公司利用479 nm光泵浦半导体激光器（OPSL）对镨晶体进行抽运，实现了输出功率为1 W的261 nm激光[13]。2011年，Gün等[14]使用激光二极管（LD）泵浦Pr^{3+}:$LiYF_4$，通过腔内倍频获得了481 mW的261.3 nm深紫外激光输出。2022年，李昕奇等[15]将Pr^{3+}:$LiYF_4$作为激光晶体，通过BBO腔内倍频获得了最大功率为110 mW的单纵模261 nm连续深紫外激光输出。2012年，Rahman等[16]报道了抗抑郁药物盐酸舍曲林在不同条件下的水解情况，他们使用探测波长为273 nm的反相高效液相色谱法（RP-HPLC）测量了舍曲林的含量。笔者测量了室温下Pr^{3+}:$LiYF_4$晶体的偏振发射光谱，发现除常见的跃迁波长外，测试的荧光谱线中出现了$^3P_0\rightarrow{}^3H_5$跃迁对应的弱荧光谱线，其波长为546 nm。近期，本课题组选用双端泵浦Pr^{3+}:$LiYF_4$晶体的方式，利用BBO晶体将此弱谱线倍频，获得了功率为128 mW的273 nm连续深紫外激光[17]。单频激光器相较于普通固体激光器具有谱线窄、相干性好等优点，已被广泛应用于拉曼光谱、全息技术等领域。为了进一步探究273 nm深紫外激光，本课题组在实验光路中加入选模元件，成功获得了中心波长为272.93515 nm的单纵模深紫外激光，其最大输出功率为32 mW。

2 实验设计

2.1 泵浦用LD的选择

图1[18]是掺杂浓度为0.5%的Pr^{3+}:$LiYF_4$晶体在室温下的吸收谱线，其峰值波长分别为441 nm（σ偏振）、444 nm（π偏振）、469 nm（π偏振）和479 nm（π偏振）。综合分析图1和表1[19-20]可知，$^3H_4\rightarrow{}^3P_2$跃迁所对

收稿日期：2023-02-14；**修回日期**：2023-03-13；**录用日期**：2023-04-25；**网络首发日期**：2023-05-06

基金项目：吉林省重点研发计划（20230201062GX）

通信作者：*douniweixiao@163.com

应的峰值波长为444 nm的泵浦光有足够大的吸收截面(9.0×10^{-20} cm^2)和较大的吸收带线宽(1.8 nm)。当利用π偏振的444 nm LD泵浦时,Pr^{3+}:$LiYF_4$晶体对泵浦光的吸收效率能够达到最高,适合蓝光LD泵浦。$^3H_4$→$^3P_0$跃迁对应的峰值波长为479 nm的泵浦光的吸收截面最大,为2.17×10^{-19} cm^2,但吸收带线宽仅为0.5 nm。若利用此吸收带进行泵浦,则对泵浦源的波长准确性要求较高,而且线宽需较窄。目前,479 nm激光器是光泵浦半导体激光器,成本较高。$^3H_4$→$^3P_1$+$^1I_6$跃迁对应的峰值波长为469 nm的泵浦光的吸收截面和吸收线宽(0.9 nm)均不高,而且单管LD功率不高。相比较而言,Pr^{3+}:$LiYF_4$晶体对峰值波长为441 nm(σ偏振)的泵浦光与469 nm(π偏振)、479 nm(π偏振)泵浦光有着相近的吸收系数,但其对441 nm(σ偏振)的泵浦光有着更宽的吸收带线宽(1.8 nm)。另外,本课题组测量了Pr^{3+}:$LiYF_4$晶体对π偏振的444 nm波长的吸收效率(约94%),同时对比了Pr^{3+}:$LiYF_4$晶体对441 nm和444 nm两个波长的吸收效率,结果显示:对441 nm波长的吸收效率(约79.5%)要高于对444 nm波长的吸收效率(约53%)。

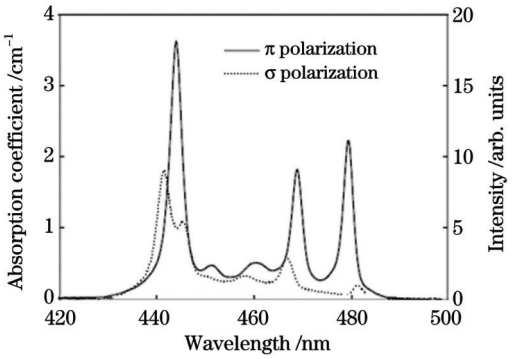

图1　Pr^{3+}:$LiYF_4$晶体的吸收谱线

Fig. 1　Absorption spectra of Pr^{3+}:$LiYF_4$ crystal

表1　Pr^{3+}:$LiYF_4$晶体蓝光波段的峰值吸收截面(室温)

Table 1　Peak absorption cross section of blue light in Pr^{3+}:$LiYF_4$ crystal (room temperature)

Peak wavelength λ /nm	Absorption cross section σ_a /(10^{-20}cm^2)	Polarization	Corresponding transition	Line width Δλ /nm
441	4.1	σ	$^3H_4$→$^3P_2$	1.8
444	9.0	π	$^3H_4$→$^3P_2$	1.8
469	6.5	π	$^3H_4$→$^3P_1$+$^1I_6$	0.9
479	21.7	π	$^3H_4$→$^3P_0$	0.5

在Pr^{3+}:$LiYF_4$晶体的三个主要吸收波段中,444 nm波段的LD生产工艺相对比较成熟,更商业化,比较适合作为抽运源。此外,Pr^{3+}:$LiYF_4$晶体对光的吸收具有偏振特性,所以将两个不同吸收波长的LD进行偏振合光后作为抽运源,既能使整体抽运功率提高,又能保留抽运光的偏振特性,从而使晶体的吸收效率也相应提高。本实验中的LD选用π偏振的444 nm和σ偏振的441 nm合束作为泵浦源来提高273 nm激光的输出功率。半导体器件最重要的一个特性是温度特性,可以通过改变温度在一定程度上改变半导体激光器的波长。LD波长会随输出功率的增大而变长(如图2所示),因此实验中使用半导体制冷器(TEC)分别控制两支LD的温度,使LD的输出功率最大时,LD的波长尽量吻合晶体吸收峰。在LD允许的工作温度范围内,通过温控方法将π偏振方向LD的中心波长调节到443.9 nm,将σ偏振方向LD的中心波长调节到441.2 nm,使Pr^{3+}:$LiYF_4$晶体获得最大的吸收效率。

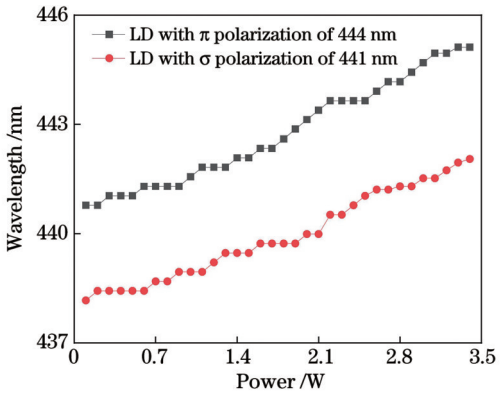

图2　LD波长随功率变化的曲线

Fig. 2　Curve of LD wavelength changing with power

2.2　实验装置

图3是室温下Pr^{3+}:$LiYF_4$晶体的偏振发射谱,

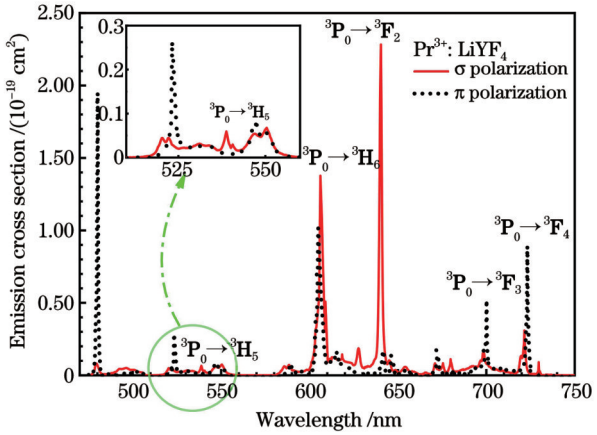

图3　Pr^{3+}:$LiYF_4$晶体的偏振发射截面

Fig. 3　Polarization-dependent emission cross section of a Pr^{3+}:$LiYF_4$ crystal (the inset shows the details of the investigated emission spectrum)

$^3P_0 \rightarrow {}^3H_5$跃迁发射弱荧光谱线，其波长为546 nm。通过腔内倍频单纵模546 nm激光获得了单纵模273 nm深紫外激光，实验装置如图4所示。两支LD分别是π偏振的444 nm蓝光二极管和σ偏振的441 nm蓝光二极管，其最大输出功率都是3.5 W。两支LD输出的光束经过焦距f=4.05 mm的透镜进行准直，再通过偏振片进行合光，然后通过焦距f=23 mm的平凸镜聚焦到工作物质Pr^{3+}:$LiYF_4$上。工作物质Pr^{3+}:$LiYF_4$的掺杂浓度为0.5%，尺寸为3 mm×3 mm×7 mm。谐振腔镜M1为晶体的入光面，膜系是440～445 nm增透膜（反射率小于0.5%）和546 nm高反膜（反射率大于99.7%）。M2是曲率半径为R=100 mm的输出镜，膜系是546 nm高反膜（反射率大于99.7%）和273 nm增透膜（反射率小于15%）。BBO晶体的尺寸为2 mm×2 mm×5 mm，切割角度θ=45.9°，Φ=0°。M3是曲率半径R=600 mm的全反镜，膜系是546 nm和273 nm高反膜，反射率大于99.7%。光路内插入两个F-P标准具（FP1和FP2）。激光器内有多个制冷器（TEC）分别对两支二极管、Pr^{3+}:$LiYF_4$晶体、BBO晶体和F-P标准具进行精确控温，以保证激光器稳定运行。

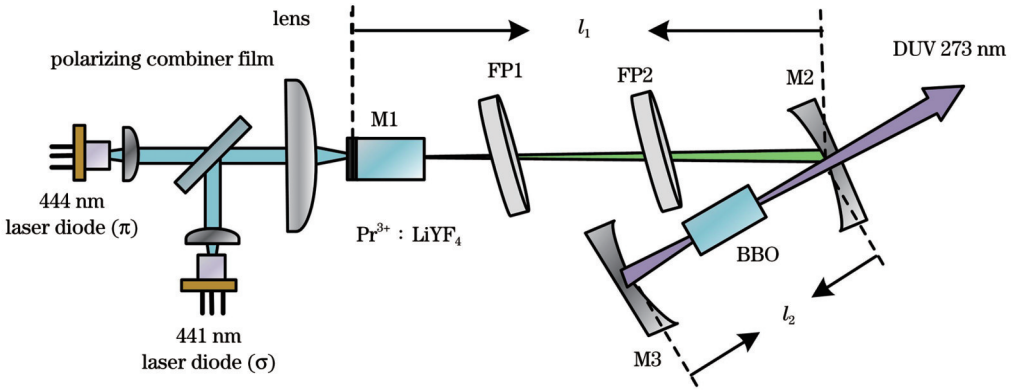

图4　全固态单纵模273 nm深紫外激光器

Fig. 4　All solid state single longitudinal mode 273 nm DUV laser

V形折叠腔内没有深紫外光通过增益材料，因此避免了深紫外光诱导降解的风险。在此谐振腔中，长臂l_1=30 mm，短臂l_2=14 mm。谐振腔内束腰半径的计算公式为

$$\omega_n = \lambda^{\frac{1}{2}} \cdot |b|^{\frac{1}{2}} \cdot \frac{1}{\pi} \cdot \left[1 - \left(\frac{a+d}{2}\right)^{\frac{1}{2}}\right]^{-\frac{1}{2}}, \tag{1}$$

式中：ω_n为谐振腔内任意一点处的束腰半径；λ为入射光波长；a、b、d为腔内光束传输矩阵中的元素。当热焦距R_{th}为−300 mm时，软件模拟得到光束在Pr^{3+}:$LiYF_4$晶体内的束腰半径ω_1约为69 μm，在BBO晶体中的束腰半径ω_2约为102 μm，如图5(a)所示。Pr^{3+}:$LiYF_4$晶体中的束腰相对较小，以保证激发效率；BBO晶体中的束腰相对较大，以降低深紫外光的功率密度，减小对晶体的损伤。图5(b)是谐振腔稳定性的二维模拟图，其中d_2为Pr^{3+}:$LiYF_4$晶体增透膜端面到输出镜的距离，d_3为输出镜到BBO（靠近输出镜一端）的距离，谐振腔处在浅蓝色区域（稳定性约为−0.3），代表该谐振腔结构的选择是合适的，在腔内能够形成稳定振荡的高斯光束。此外，谐振腔设计处于浅蓝色的中间区域，腔长有较宽的稳定范围，不易受温度、应力及振动等因素的影响。

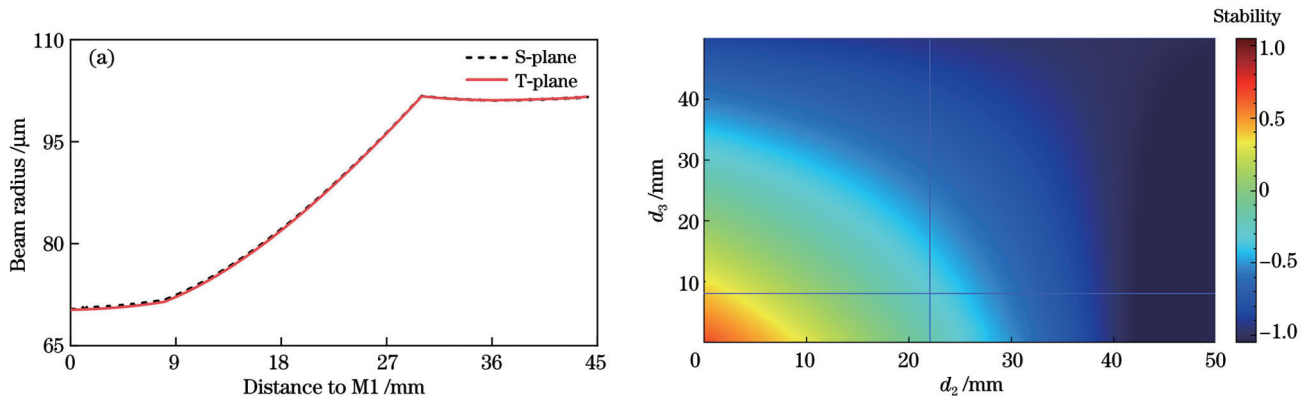

图5　谐振腔分析。(a)谐振腔内束腰半径模拟图；(b)谐振腔稳定性模拟图

Fig. 5　Stability analysis of resonant cavity. (a) Simulation of beam waist radius in the resonant cavity; (b) simulation of stability map in the resonant cavity

本实验装置同时使用两个不同的F-P标准具组合进行纵模选取。两个F-P标准具分别是厚度D_1=1.2 mm、反射率R_1=70% 以及厚度D_2=0.5 mm、反射率R_2=60% 的熔融石英标准具，入射角(α_1、α_2)均为0.25°。根据经验，一般固体激光器的线宽小于0.25 nm，因此本课题组模拟了0.25 nm增益带宽内的纵模透过率。从图6(a)中可以看出，除了主峰以外，相邻纵模的透过率都在50% 以下，已经不能形成稳定的纵模输出，只需要考虑主峰内的纵模情况。根据谐振腔长，可以计算出纵模间隔为2.34 GHz(0.00233 nm)。光束以小角度入射到标准具组时，可以得到标准具组对不同纵模的透过率曲线，如图6(b)所示。当其中一个纵模的透过率最大(透过率T=100%)时，相邻纵模的透过率小于80%，表示标准具组对相邻纵模有20% 的损耗。以上损耗均为单次透过损耗。谐振腔内的纵模反射次数会达到上万次，实际上的损耗是极大的，只有在T=100% 处的单个纵模可以起振，从而保证激光器的单纵模输出。

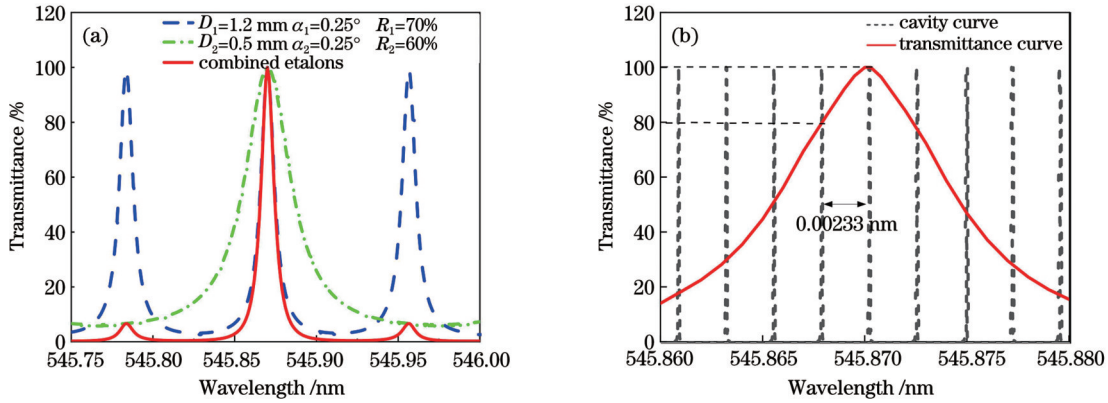

图6　F-P标准具的透过率。(a)0.25 nm范围内两F-P标准具组的透过率；(b)0.02 nm范围内两F-P标准具组的透过率

Fig. 6　Transmittance of F-P etalon. (a) Combined transmittance of two F-P etalons in the range of 0.25 nm; (b) combined transmittance of two F-P etalons in the range of 0.02 nm

3　实验结果与分析

当腔内不加任何选模元件时，获得了输出功率为85 mW的273 nm深紫外激光，测量结果为多个纵模。加入两个标准具后，可以输出32 mW的单纵模激光，此时利用波长计(High Finesse WS7)测量单纵模273 nm激光光谱，测量结果如图7所示。可见：波长单一，没有相邻纵模。中心波长为272.93515 nm，光谱线宽小

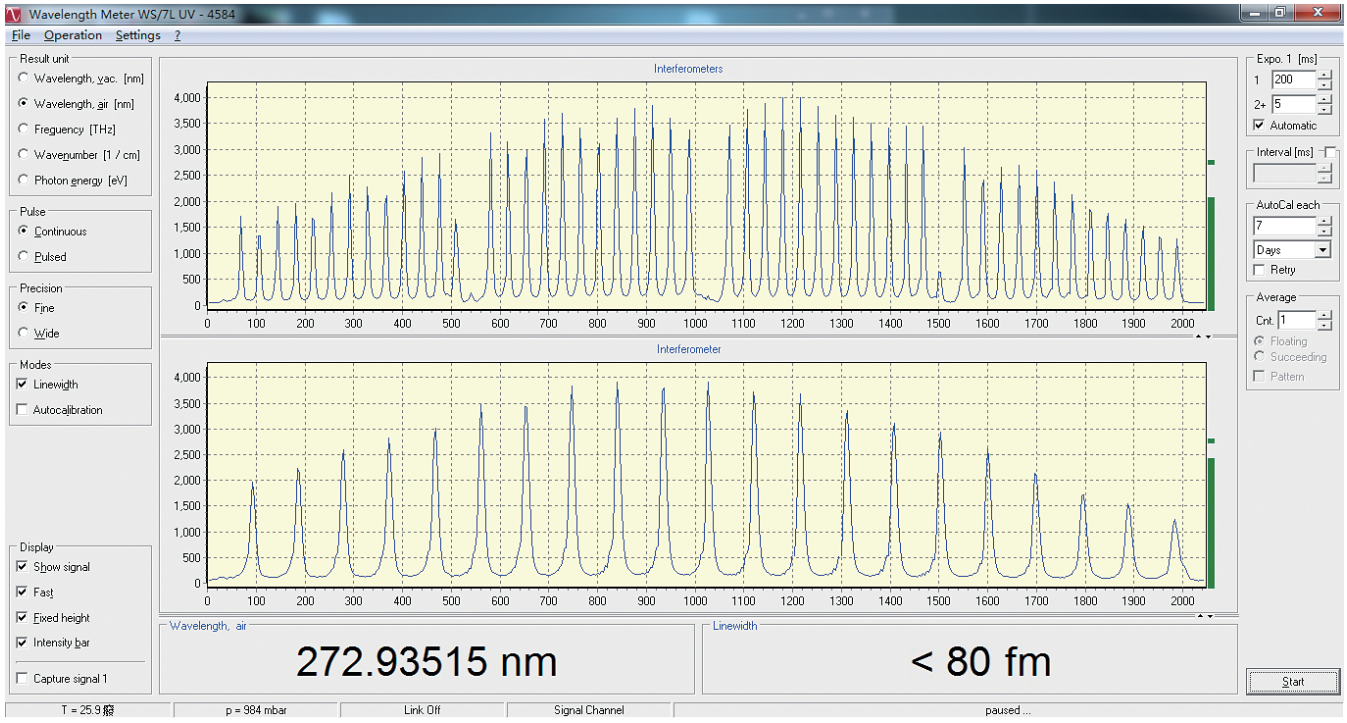

图7　波长及线宽测试图

Fig. 7　Test diagram of wavelength and linewidth

于 80 fm。此外，测量了 2 h 波长稳定性，波长总变化量为 4.5 pm，如图 8 所示。

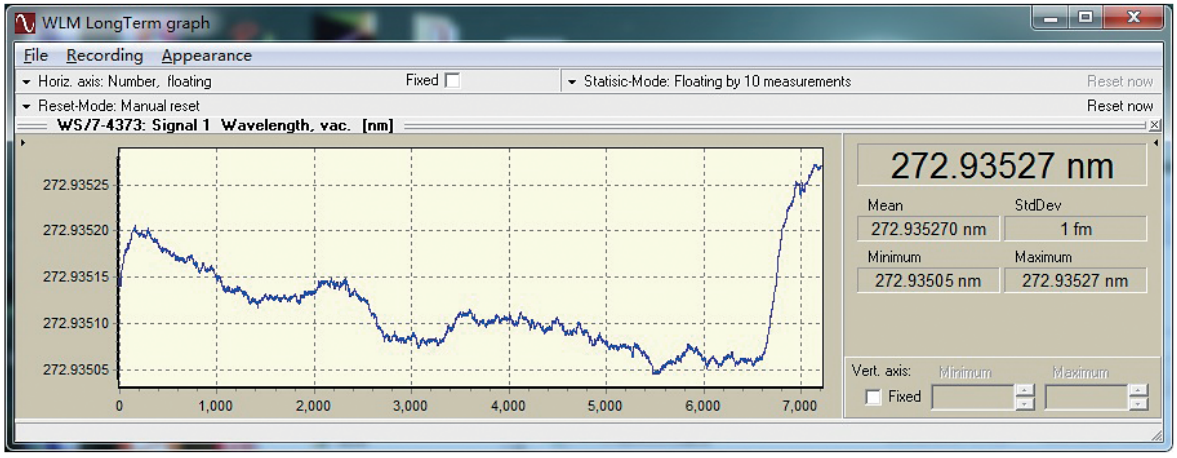

图 8　2 h 波长稳定性测试图

Fig. 8　Test diagram of wavelength stability in 2 h

利用功率计（Coherent FieldMaxII-TO）测量单纵模 273 nm 深紫外激光的输出功率。当 441 nm 和 444 nm 两支 LD 组合输出功率为 6240 mW 时，获得了 273 nm 单纵模激光的最大输出功率（32 mW）。根据实验测试结果，得到了激光的输出特性拟合曲线，如图 9 所示。273 nm 单纵模深紫外激光输出功率随着泵浦功率的增大呈上升趋势，斜率也有变大的趋势，这应该是 LD 波长逐步调整到 Pr^{3+}:$LiYF_4$ 晶体吸收峰所致。而后，随着泵浦功率持续增大，LD 波长逐渐偏离晶体吸收峰而且晶体热透镜效应加剧，曲线斜率逐渐变得平缓，测试结果与图 2 相吻合。此外，测量了单纵模 273 nm 深紫外光最大功率的稳定性，连续测试 1 h，均方根（RMS）功率稳定性为 0.717%（如图 9 插图所示）。未观察到深紫外线引起的退化或泵浦激光功率下降的迹象。

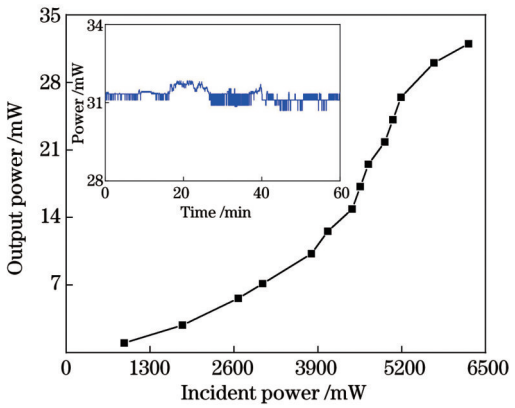

图 9　单纵模 273 nm 深紫外激光的输出功率特性以及 273 nm 激光 1 h 功率稳定性测试图

Fig. 9　Output power characteristic of single longitudinal mode 273 nm deep UV laser & power stability of 273 nm laser in 1 h

图 10 是在满功率 32 mW 时测量的光斑及光束质量因子 M^2。图 10(a)为光斑轮廓分析仪（Spiricon BM-USB-SP928-IOS）测量的远场光斑形貌，由于 BBO 晶体的走离效应，激光光斑为长条状。图 10(b)是使用光束质量分析仪（Thorlabs BP209-VIS/M）测得的光束质量因子 M^2，其在 X 轴方向为 2.29，在 Y 轴方向为 2.21。

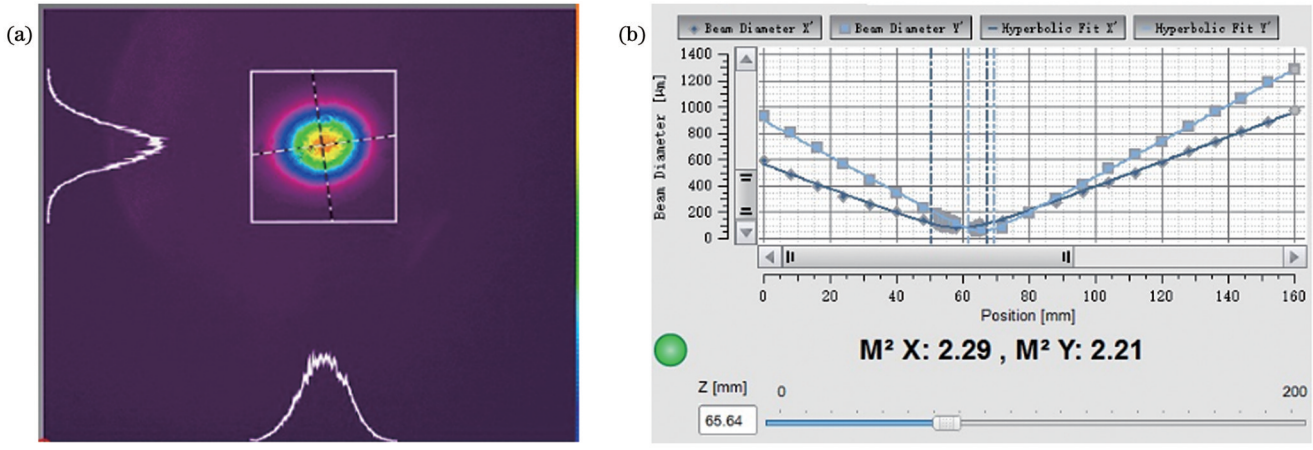

图 10　273 nm 激光横模特征图片。(a)光斑图；(b)光束质量因子 M^2 测试图

Fig. 10　273 nm laser transverse mode characteristic photos. (a) Laser beam; (b) measured beam quality factor M^2

4 结 论

选用国产 Pr^{3+}:$LiYF_4$晶体作为激光增益介质,设计了简单有效的V形折叠腔,利用π偏振、中心波长为444 nm的LD以及σ偏振、中心波长为441 nm的LD的偏振合光作为泵浦源,使用两个不同的F-P标准具组合对腔内纵模进行选取,通过BBO晶体倍频546 nm基频光,实现了稳定运转的273 nm单纵模深紫外激光器。该激光器的中心波长为272.93515 nm,最大输出功率为32 mW,连续测量1 h的RMS功率稳定性为0.717%。本实验选取的泵浦源可以很好地匹配晶体的吸收峰,使吸收效率最大化,提高了激光输出功率。下一步本课题组将继续优化谐振腔,增加注入泵浦光的功率,进一步提高273 nm单纵模深紫外激光的输出功率。

参 考 文 献

[1] Kaneda Y, Yarborough J M, Merzlyak Y, et al. Continuous-wave, single-frequency 229 nm laser source for laser cooling of cadmium atoms[J]. Optics Letters, 2016, 41(4): 705-708.

[2] Yang G H, Wu H M, Pembere A M S, et al. Deep ultraviolet laser radiation causes brittle fracture of Cα-Cβ bonds in neurotransmitters[J]. Chemistry Select, 2019, 4(18): 5235-5239.

[3] Ning Y X, Li Y F, Wang C, et al. Tunable deep ultraviolet laser based near ambient pressure photoemission electron microscope for surface imaging in the millibar regime[J]. The Review of Scientific Instruments, 2020, 91(11): 113704.

[4] Zhang Y, Liu Q X, Fu X H, et al. A stable deep-ultraviolet laser for laser cooling of mercury atoms[J]. Optics & Laser Technology, 2021, 139: 106956.

[5] Sakuma J, Asakawa Y, Obara M. Generation of 5-W deep-UV continuous-wave radiation at 266 nm by an external cavity with a $CsLiB_6O_{10}$ crystal[J]. Optics Letters, 2004, 29(1): 92-94.

[6] Wang G L, Geng A C, Bo Y, et al. 28.4 W 266 nm ultraviolet-beam generation by fourth-harmonic generation of an all-solid-state laser[J]. Optics Communications, 2006, 259(2): 820-822.

[7] 赵彪, 秦玮霞, 李凤琴, 等. 全固态连续单频266 nm深紫外激光器[J]. 量子光学学报, 2020, 26(2): 194-201.
Zhao B, Qin W X, Li F Q, et al. All-solid-state CW single-frequency deep UV 266 nm laser[J]. Acta Sinica Quantum Optica, 2020, 26(2): 194-201.

[8] Zimmermann C, Vuletic V, Hemmerich A, et al. All solid state laser source for tunable blue and ultraviolet radiation[J]. Applied Physics Letters, 1995, 66(18): 2318-2320.

[9] Deyra L, Martial I, Didierjean J, et al. Deep-UV 236.5 nm laser by fourth-harmonic generation of a single-crystal fiber Nd: YAG oscillator[J]. Optics Letters, 2014, 39(8): 2236-2239.

[10] Goldberg L, Kliner D A V. Deep-UV generation by frequency quadrupling of a high-power GaAlAs semiconductor laser[J]. Optics Letters, 1995, 20(10): 1145-1147.

[11] Xu B, Camy P, Doualan J L, et al. Visible laser operation of Pr^{3+}-doped fluoride crystals pumped by a 469 nm blue laser[J]. Optics Express, 2011, 19(2): 1191-1197.

[12] Luo S Y, Yan X G, Xu B, et al. Few-layer Bi_2Se_3-based passively Q-switched Pr: YLF visible lasers[J]. Optics Communications, 2018, 406: 61-65.

[13] Ostroumov V, Seelert W, Clarkson W A, et al. 1 W of 261 nm cw generation in a Pr^{3+} : $LiYF_4$ laser pumped by an optically pumped semiconductor laser at 479 nm[J]. Proceedings of SPIE, 2008, 6871: 68711K.

[14] Gün T, Metz P, Huber G. Efficient continuous wave deep ultraviolet Pr^{3+} : $LiYF_4$ laser at 261.3 nm[J]. Applied Physics Letters, 2011, 99(18): 181103.

[15] 李昕奇, 浦双双, 牛娜, 等. 单纵模261 nm紫外激光器的研制[J]. 中国激光, 2022, 49(9): 0901002.
Li X Q, Pu S S, Niu N, et al. Development of 261 nm single-longitudinal mode ultraviolet laser[J]. Chinese Journal of Lasers, 2022, 49(9): 0901002.

[16] Rahman M A, Hussain A, Iqbal Z, et al. Estimation of sertraline by chromatographic (HPLC-UV273 nm) technique under hydrolytic stress conditions[J]. Pharmaceutical Methods, 2012, 3(2): 62-67.

[17] Dou W, Pu S S, Qu D P, et al. Generation of continuous wave deep UV radiation at 273 nm based on frequency doubling of a diode pumped PR: YLF laser[J]. Applied Physics B, 2023, 129(2): 30.

[18] 牛娜, 曲大鹏, 窦微, 等. 蓝光二极管抽运掺镨氟化钇锂晶体腔内倍频348.9 nm紫外激光器[J]. 中国激光, 2018, 45(12): 1201003.
Niu N, Qu D P, Dou W, et al. 348.9 nm intra-cavity frequency-doubling ultraviolet laser in blue laser diode pumped Pr: YLF crystal[J]. Chinese Journal of Lasers, 2018, 45(12): 1201003.

[19] Iijima K, Kariyama R, Tanaka H, et al. Pr^{3+}: YLF mode-locked laser at 640 nm directly pumped by InGaN-diode lasers[J]. Applied Optics, 2016, 55(28): 7782-7787.

[20] 霍晓伟, 齐瑶瑶, 李宇琪, 等. LD泵浦掺Pr^{3+}的可见光固体激光器研究进展[J]. 光电技术应用, 2019, 34(5): 7-15.
Huo X W, Qi Y Y, Li Y Q, et al. Research progress of LD-pumped Pr^{3+}-doped solid-state laser in visible wavelength[J]. Electro-Optic Technology Application, 2019, 34(5): 7-15.

Development of All Solid State Single Longitudinal Mode 273 nm Deep-Ultraviolet Laser

Dou Wei[1], Hou Shanshan[1], Zheng Zhiyuan[1], Yu Bowei[1], Chen Xi[1], Zheng Quan[1,2*]

[1]*Changchun New Industries Optoelectronics Technology Co., Ltd., Changchun* 130103, *Jilin, China*;

[2]*Changchun Institute of Optics, Fine Mechanics and Physics, Chinese Academy of Sciences, Changchun* 130033, *Jilin, China*

Abstract

Objective The features of deep-ultraviolet lasers are high single-photon energy, short wavelength, and easy absorption by materials. They are widely used in high-density optical data storage, high-resolution optical microscopy, material processing, spectral analysis, scientific research, and medical sterilization and diagnostic equipment. Currently, most deep-ultraviolet lasers are obtained by two or more nonlinear frequency conversions of near-infrared lasers; however, the efficiency of this method is generally low. In

recent years, rare-earth ions (Pr^{3+}) that can emit a visible laser directly at room temperature have attracted considerable attention. Its emission wavelengths span over the blue (485 nm), green (523 nm), orange (604 and 607 nm), and red (640, 698, and 721 nm) regions. The appearance of Pr^{3+} also makes it possible to obtain a deep-ultraviolet laser through a single nonlinear frequency conversion. Polarized emission spectra of the Pr^{3+} : $LiYF_4$ crystal were measured at room temperature. In addition to the standard transition wavelengths, a weak fluorescence spectrum of the $^3P_0 \rightarrow {}^3H_5$ transition was observed in the tested fluorescence lines at 546 nm. Recently, in our experimental group, we used a double-end-pumping Pr^{3+} : $LiYF_4$ crystal for frequency-doubling of the weak spectral line with a β-BaB_2O_4 (BBO) crystal and obtained a continuous deep-ultraviolet laser at 273 nm with a power of 128 mW. Compared to ordinary solid-state lasers, single-frequency lasers have the advantages of excellent stability, narrow spectral lines, and good coherence. This study added a mode selection element to explore the 273 nm deep-ultraviolet laser further. A single longitudinal mode deep-ultraviolet laser with a center wavelength of 272.93515 nm was successfully obtained, and the maximum output power was 32 mW. This study is essential for measuring the content of the antidepressant sertraline hydrochloride.

Methods The absorption properties of polarized Pr^{3+} : $LiYF_4$ crystals were studied. The absorption efficiency of the Pr^{3+} : $LiYF_4$ crystal at 444 nm wavelength for π polarization was measured (~94%), and the absorption efficiencies at two wavelengths for σ polarization were compared. The absorption efficiency at 441 nm (~79.5%) was higher than that at 444 nm (~53%). The absorption of laser by the Pr^{3+} : $LiYF_4$ crystal has polarization characteristics; thus, two laser diodes (LDs) of different wavelengths were combined by polarization as the pumping source. As a result, the entire pump power can be improved, and the polarization characteristics of the pump can be retained such that the absorption efficiency of the crystal correspondingly improves. Therefore, two LDs with an output power of 3.5 W, 444 nm in π-polarization direction and 441 nm in σ-polarization direction were used as the pump source; the length of Pr^{3+} : $LiYF_4$ crystal was 7 mm and that of the BBO crystal was 5 mm for intracavity frequency doubling. A V-shaped folded cavity was designed (Fig. 4). The beam waist radius (69 um) in Pr^{3+} : $LiYF_4$ crystal was designed to be small to ensure absorption efficiency. In contrast, the beam waist radius (102 μm) in BBO crystal was designed to be relatively large to reduce the power density of deep-ultraviolet laser and damage to the crystal (Fig. 5). Simultaneously, two different Fabry-Perot (F-P) etalon combinations were used to select the longitudinal mode. Two F-P etalons, with thickness of 0.5 mm and 1.2 mm and reflectivity of 60% and 70%, respectively, were selected with an incident angle of 0.25°. According to the cavity length, the longitudinal mode interval was calculated to be 2.34 GHz (0.00233 nm). The transmittance curves of the etalon sets were simulated for different longitudinal modes when the beam was incident at a small angle. When one of the longitudinal modes had the maximum transmittance (T=100%), the adjacent longitudinal mode exhibited a single-transmission loss of approximately 20% (Fig. 6). Under the condition that the longitudinal mode in the resonant cavity oscillates and is lost multiple times, only a single longitudinal mode at T=100% can initiate the oscillation, thereby ensuring a single longitudinal mode output of the laser.

Results and Discussions Without any mode selector in the cavity, a deep-ultraviolet laser at 273 nm with an output power of 85 mW was obtained, and the measured results were multiple longitudinal modes. After adding two etalons, the single longitudinal mode 273 nm laser spectrum was measured using a wavelength meter (High Finesse WS7). The wavelength was single, and there was no adjacent longitudinal mode. The center wavelength was 272.93515 nm, the spectral linewidth was less than 80 fm (Fig. 7), and the wavelength stability was measured for two hours at a wavelength variation of 4.5 pm(Fig. 8). The output power of a single longitudinal mode deep-ultraviolet laser at 273 nm was measured using a power meter (Coherent FieldMaxII-TO). The maximum output power of a single longitudinal mode deep-ultraviolet laser at 273 nm (32 mW) was obtained when the combined output power of the two LDs at 441 and 444 nm was 6240 mW. The curve of the laser output characteristics was fitted to the experimental results. The output power of the single longitudinal mode deep-ultraviolet laser at 273 nm increases with increasing pump power. The slope also tends to increase potentially owing to the gradual adjustment of the LD wavelength to the absorption peak of the Pr^{3+} : $LiYF_4$ crystal. As the pump power continues to increase, the LD wavelength gradually deviates from the absorption peak of the crystal, the thermal lens effect of the crystal intensifies, and the slope of the curve gradually flattens (Fig. 9). We used a coherent power meter to test the stability of the maximum power of a single longitudinal mode 273 nm deep-ultraviolet laser. The root-mean-square (RMS) of the power stability was 0.717% after 1 h of continuous testing (Fig. 9). We measured the far-field beam shape using a beam profile analyzer (Spiricon BM-USB-SP928-IOS), which was a long strip owing to the walk-off effect of the BBO crystal. The beam quality (M^2 factor) was measured as 2.29 in the X- and 2.21 in the Y- direction using a beam quality analyzer (Thorlabs BP209-VIS/M) (Fig. 10).

Conclusions In this study, a simple and effective V-shaped folded cavity was designed using a Pr^{3+} : $LiYF_4$ crystal made in China as the laser gain medium, and a π-polarized laser with a center wavelength of 444 nm and a σ-polarized laser with a center wavelength of 441 nm were used as the pump sources. Two different F-P etalons were used to select the longitudinal mode in the cavity, and the BBO crystal doubled the fundamental frequency of 546 nm to realize the stable operation of a 273 nm single longitudinal mode deep-ultraviolet laser. The measured center wavelength is 272.93515 nm, the maximum output power is 32 mW, and the RMS power stability is 0.717% in a 1 h continuous measurement. The pump source selected in this experiment matches the absorption peak of the crystal well, maximizes the absorption efficiency, and improves the laser output power. In future, we plan to continue to optimize the resonator, increase the power of the injected pump light, and further improve the output power of the 273 nm single longitudinal mode deep-ultraviolet laser.

Key words lasers; deep-ultraviolet laser; single-longitudinal mode; Pr^{3+} : $LiYF_4$ crystal; Fabry-Perot etalon